Advances in Geo-Energy Research

Vol. 15, No. 2, p. 99-111, 2025

Original article

Design of passive insulation system and optimization of thermal insulation material for deep *in-situ* condition-preserved coring

Jianping Yang[1,2,3], Haishu Bai[4], Zhiqiang He[2,5]*, Bo Yu[4], Heping Xie[1,2,3]

[1] *College of Polymer Science and Engineering, Sichuan University, Chengdu 610065, P. R. China*

[2] *State Key Laboratory of Intelligent Construction and Healthy Operation and Maintenance of Deep Underground Engineering, Sichuan University, Chengdu 610065, P. R. China*

[3] *Institute of Deep Earth Sciences and Green Energy, College of Civil and Transportation Engineering, Shenzhen University, Shenzhen 518060, P. R. China*

[4] *School of Mechanical Engineering, Sichuan University, Chengdu 610065, P. R. China*

[5] *College of Water Resource & Hydropower, Sichuan University, Chengdu 610065, P. R. China*

Keywords:
Deep *in-situ* conditions
coring device
passive insulation system
thermal insulation material
epoxy resin

Cited as:
Yang, J., Bai, H., He, Z., Yu, B., Xie, H. Design of passive insulation system and optimization of thermal insulation material for deep *in-situ* condition-preserved coring. Advances in Geo-Energy Research, 2025, 15(2): 99-111.
https://doi.org/10.46690/ager.2025.02.03

Abstract:
In order to help establish a new theory of deep rock mechanics and better guide the development of deep engineering, it is crucial to develop a deep *in-situ* condition-preserved coring device capable of obtaining cores while maintaining their original *in-situ* temperature and pressure conditions. To achieve insulation functionality within a compact design, a passive insulation system must be developed for such coring devices. Considering the size constraints and thermal insulation requirements, a passive thermal insulation system combining a vacuum layer and an insulating material layer has been designed in this work. Epoxy resin was selected as the insulation material due to its high compressive strength and low thermal conductivity. The type and dosage of curing agents, as well as the curing process with epoxy resin, were optimized. The ideal resin achieved a compressive strength of 241.03 MPa and a thermal conductivity as low as 0.25 W/m·K. Additionally, it exhibited excellent thermal stability and a high decomposition temperature. Under high-temperature and high-pressure water conditions simulating deep-earth environments, the epoxy resin's maximum water absorption was below 0.7%. The insulation layer could effectively minimize heat exchange between the core and the external environment by up to 19.01%. These findings provide a significant contribution to the advancement of passive insulation systems for deep *in-situ* core drilling operations.

1. Introduction

The global energy development strategy is still built on oil, coal, natural gas, and other fossil fuels as the main energy sources. However, shallow strata resources are being rapidly depleted, and the exploration of deeper underground resources is gaining increasing momentum (Wang et al., 2022, Xue et al., 2024). Despite this fact, fundamental research supporting the exploitation of deep strata resources remains inadequate. Traditional mining science and rock mechanics theories are based on 'ordinary cores' that no longer retain *in-situ* temperature, pressure and other conditions, hence they fail to effectively guide deep resource exploration or resolve the technical challenges of deep resource mining (Kong et

*Corresponding author.
E-mail address: yangjianping929@126.com (J. Yang); haishubai@163.com (H. Bai); hzqscu@scu.edu.cn (Z. He); 18981946636@163.com (B. Yu); xiehp@scu.edu.cn (H. Xie).
Yandy Scientific Press
2207-9963 © The Author(s) 2024.
Received November 6, 2024; revised December 1, 2024; accepted December 25, 2024; available online December 29, 2024.

al., 2023). The concept of deep *in-situ* condition-preserving coring, aimed at obtaining a 'fidelity core' that retains the *in-situ* temperature and osmotic pressure of deep strata, has already been proposed (Xie et al., 2024). This enables the exploration of the physical and mechanical properties of deep rocks under real subsurface conditions.

In general, the temperature in the Earth's crust increases by 3 °C for every 100 m increase in depth (Liang et al., 2005). Temperature significantly impacts rock properties and permeability, as high temperatures can induce changes in the microstructure, affecting pore connectivity and fluid flow. Saif et al. (2017) utilized computed tomography scans to observe the development of interconnected pores and fractures in oil shale exposed to high temperatures. These changes, including the increase in porosity and permeability, are essential for understanding fluid flow during oil shale pyrolysis. Furthermore, Zhao et al. (2012) reported a substantial increase in the porosity of oil shale samples from Daqing and Yan'an under temperatures ranging from 100 to 200 °C. These parameters, such as porosity, permeability and other reservoir rock characteristics, directly influence the accurate evaluation of oil and gas resources (Zhou et al., 2010). To preserve the *in-situ* temperature of deep cores, it is essential to develop coring devices that preserve temperature effectively, such as those utilizing a passive thermal insulation system. The temperature-preserved coring device is crucial for preserving the *in-situ* conditions of deep cores. In this context, the concept of combining passive and active insulation techniques has been proposed (Xie et al., 2021).

Temperature-preserved coring has mostly been applied to low-temperature seabed sediments, while deep rock formations in high-temperature environments have seen limited application. Inada and Koji (2015) designed a temperature-preserved coring device that uses air interlayers and semiconductor refrigeration to maintain the low temperature of the core. Zhu et al. (2013) developed a double-layer vacuum structure and added heat-insulating and anti-ultraviolet layers to improve the temperature preservation ability. Zang et al. (2007) applied a similar approach to develop a natural gas hydrate deep-water submersible core drilling tool. Yang et al. (2021) highlighted that reinforcing the vacuum insulating layer to withstand high-temperature and high-pressure environments significantly increases both the size and cost of the coring device. To address the size constraints of the coring device, this study employs a passive temperature-preserved coring system that integrates a vacuum layer with optimized insulation materials.

Many inorganic thermal insulation materials, such as foam glass and asbestos board, are unsuitable for passive insulation due to their loose texture, porous characteristics, brittleness, and easy water absorption. Epoxy resins, known for their high compressive strength, low thermal conductivity, and excellent thermal stability due to their dense, random cross-linking networks as thermosetting materials, are ideal for high-temperature and high-pressure applications and were thus selected as the insulation material in this work.

Herein, a passive insulation system for the deep ICP-coring device was designed, combining a vacuum layer with an insulation material layer. High-strength epoxy resin was selected as the insulation material. To optimize its performance, the type and dosage of curing agents, as well as the curing process, were carefully adjusted. This modification resulted in a material capable of withstanding deep *in-situ* conditions, including high-temperature and high-pressure water environments, thereby improving the passive insulation capability of the ICP-coring device.

2. Structural design of the passive insulation

The cost of drilling at this depth is primarily influenced by the size of the coring device, with coring costs accounting for up to 73% of the total drilling expenses (Hossain, 2015). The drilling diameter strongly influences these costs: increasing the diameter from φ8 ½" (21.59 cm) to φ12 ¼" (31.12 cm) results in a 40% cost increase. Therefore, it is critical to minimize the diameter of the deep ICP-coring device as much as possible. The vacuum interlayer scheme is the most effective method for achieving passive insulation, but it requires an insulation layer three times thicker than that needed for high-strength passive insulation materials. On the basis of the structural design of the deep ICP-coring device and previous strength calculations by our team, a passive thermal insulation system was designed, combining a vacuum section and an insulation material section (Shi et al., 2023). The length of the vacuum insulation section is 935 mm, while that of the insulation material section is 1,105 mm, as shown in Fig. 1.

In the core cabin sleeve section, due to the large size of the core cabin and overall device size limitations, only a high-strength insulation material can meet the strength requirements for deep *in-situ* conditions. For other parts of the core cabin, the vacuum layer insulation scheme suffices to meet the strength requirements of the coring device.

3. Experimental materials and methods

3.1 Materials

The strength of epoxy resin is influenced by its structure, the curing agent used, and the curing process. Although many types of epoxy resins exist, the insulation material used in the deep ICP-coring device must be formed within the ring cavity of the core picker, which requires a specific structure. The diglycidyl ether of bisphenol A epoxy, E51, meets these requirements as (1) it is a low-viscosity liquid before curing and (2) it achieves high strength after curing (Moller et al., 2020). Thus, E51 was selected as the epoxy resin prepolymer. To ensure compatibility with the complex coring structure, the epoxy must be in liquid form prior to curing. The curing agent plays a crucial role in determining the strength of epoxy resin (Kumar and Srivastava, 2017). On the basis on the main chain structure of E51 and the distribution of epoxy groups, four curing agents were selected: 594 boramine curing agent, diethyltetramethylimidazole (2E4MI), aminoethylethanolamine (AEEA), and meta-phenylenediamine (*m*-PDA). Although through different reaction mechanisms, each curing agent interacts with E51.

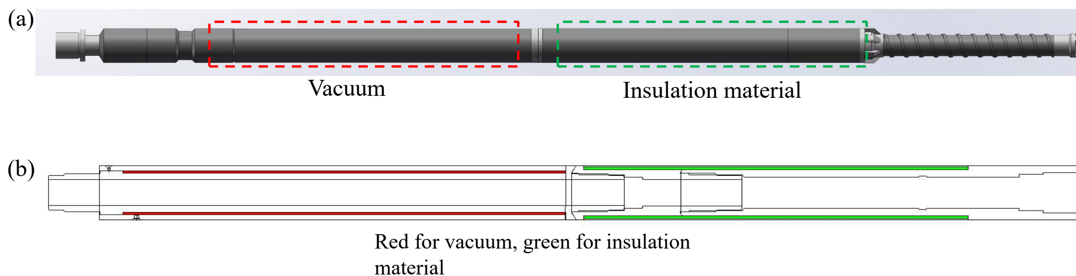

Fig. 1. Passive insulation for ICP-coring device. (a) schematic model of the deep icp-coring device (excerpt) and (b) schematic of passive insulation.

Table 1. Curing parameters for different curing agents.

Curing agent	Curing agent: E51 (wt.%)	Curing process
594	10	0.5 h at 170 °C and 2 h at 150 °C
AEEA	16	4 h at 100 °C
2E4MI	7	1 h at 80 °C and 3 h at 170 °C
m-PDA	10	4 h at 80 °C, 2 h at 150 °C and 3 h at 180 °C

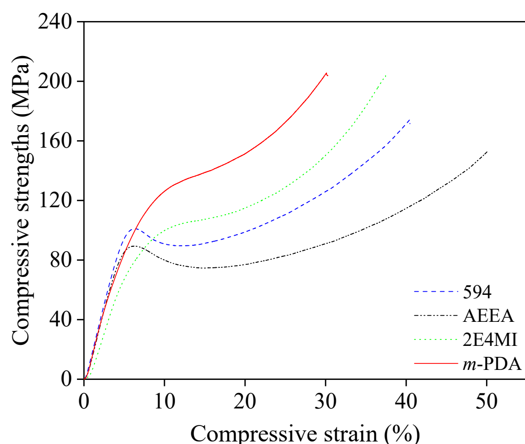

Fig. 2. Compressive strengths of the epoxy resin with different curing agents used.

3.2 Preparation of epoxy resin

The preparation of the epoxy resin involved several key steps. First, the required amounts of curing agent (*m*-PDA as an example) and epoxy resin E51 were accurately measured. Next, the epoxy resin E51 and the curing agent were thoroughly stirred to achieve a uniform mixture. Then, the curing temperature was set and the heating and curing process was initiated. At this stage, both the epoxy resin E51 and the curing agent consisted of small molecular structures. Finally, the curing process was completed, resulting in cross-linking between the epoxy E51 and the curing agent, which formed a random network structure and yielded the solid epoxy matrix.

3.3 Curing agent optimization

The components were carefully weighed according to the specified ratios and the curing agent was uniformly blended with E51 epoxy resin to form a homogeneous prepolymer mixture. This mixture was then poured into a mold and subjected to a controlled heating process in an oven to ensure optimal curing conditions, as detailed in Table 1.

3.3.1 Curing agent optimization

The *m*-PDA-E51 system exhibited the highest compressive strength, as illustrated in Fig. 2. In contrast, both the 594-E51 and AEEA-E51 systems initially entered the elastic deformation stage, transitioned into the strain weakening stage, and finally entered the strain strengthening stage. The *m*-PDA-E51 and 2E4MI-E51 systems, on the other hand, underwent elastic deformations and directly moved into the strain strengthening stage without significant strain weakening. When the compressive strain was less than 5%, the compressive strength of the epoxy resins remained similar. However, as the compressive strain increased, the compressive strength reached its maximum at 10% and 20% strain, with the *m*-PDA-E51 system showing superior performance, as shown in Table 2. Notably, as Fig. 2 indicates, under the same compressive strain, the *m*-PDA-E51 system demonstrated higher compressive strength than the 2E4MI-E51 system. Additionally, although the Young's modulus during elastic deformation was slightly higher for the 594-E51 and AEEA-E51 systems compared to the *m*-PDA-E51 system, their maximum compressive strengths were considerably lower. Based on these findings, *m*-PDA was selected as the curing agent for the epoxy resin E51 to achieve enhanced compression performance. The curing parameters, including temperature and time, were further optimized for the *m*-PDA-E51 system, resulting in an epoxy resin with improved overall performance, which was then used as the matrix for the passive thermal insulation material.

Table 2. Compressive strength of epoxy resin.

Curing agent	Compressive strength (MPa)		
	Strain 5%	Strain 10%	Strain 20%
594	94.36	90.81	98.81
AEEA	85.26	79.96	77.01
2E4MI	67.13	99.837	114.95
m-PDA	84.30	126.16	151.32

3.3.2 Curing process optimization

The ratio of *m*-PDA/E51, the curing reaction temperature and time all affected the formation of the cross-linking structure and the chain segment of the epoxy resin, in turn impacting the strength (Vashisth et al., 2018; Moller et al., 2020). On the basis of the mechanism of the reaction of *m*-PDA with E51, the theoretical ratio of *m*-PDA/E51 was 0.13 wt.% (El Gazzani et al., 2016). Considering the reaction characteristics and steric effects of the characteristic groups in E51 and *m*-PDA, different curing agent proportions for the experimental groups were set, such as 7, 8, 9, 10, 11, 12, 13, 14, 15, and 16 wt.%. To investigate the impact of temperature on the curing degree and mechanical properties of epoxy resin, different pre-curing temperatures, post-curing temperatures and curing times were set. Subsequently, the curing process with the most favorable overall performance was chosen. The curing temperature of different stages was obtained by DSC analysis during the epoxy resin curing process. The study encompassed four distinct curing stages: (I) 4 h at 60 °C and 20 h at 80 °C, (II) 4 h at 80 °C, 2 h at 150 °C and 3 h at 180 °C, (III) 3.5 h at 50 °C, 12 h at 80 °C and 3.5 h at 180 °C, (IV) 3.5 h at 50 °C and 2 h at 80 °C. Therefore, each curing agent ratio was tested in four experimental groups at different curing temperatures, yielding a total of 40 experimental groups, each having distinct combinations of curing agent ratios and curing temperatures. In this way, the researchers prepared a series of epoxy resin samples and characterized their properties.

3.4 Characterization methods

1) Fourier Transform Infrared (FTIR) spectroscopy: This technique was used to determine the degree of the curing reaction. FTIR spectra were recorded in transmission mode using an Invenior infrared spectrometer (Bruker, United States), and the wavenumber range was 4,000 to 400 cm^{-1}.
2) Thermogravimetry (TG): This method was used to characterize the thermal decomposition temperature of the epoxy resin using an analyzer from TA Instruments Co., Ltd. (United States). Temperature range: 25 to 800 °C, heating rate: 10 °C/min and gas condition: 50 mL/min nitrogen flow.
3) Differential scanning calorimetry (DSC): This technique was applied to represent changes in the heat capacity of the epoxy resin with the change in temperature. DSC was performed with a DSC 1 equipment (Mettler Toledo, Switzerland). Temperature range: 25 to 230 °C, heating rate: 10 °C/min and gas condition: 50 mL/min nitrogen flow.
4) Mechanical properties: These are key properties for the epoxy resin used as a matrix for the thermal insulation material. The compressive strengths of the epoxy resins were tested using an Instron model 5967 instrument (Instron, the United Kingdom). The compression rate was 1 mm/min.
5) Dynamic thermomechanical analysis (DMA): This method was used to represent the thermal mechanical properties and glass transition temperature of the epoxy resin. DMA was performed with DMA 1 equipment (Mettler Toledo, Switzerland). Temperature range: 25 to 230 °C, heating rate: 10 °C/min and gas condition: air.
6) Thermal conductivity: This is a key index used to characterize the thermal insulation capacities of epoxy resins. The thermal conductivities of the epoxy resins were obtained by a TPS7 hot disk device (Hot Disk Co., Ltd., Sweden) using the test probe of model 5465.

3.5 Results and discussion

3.5.1 Mechanical properties

In order to optimize the curing agent to E51 ratio, curing temperature and curing time, epoxy resin samples with *m*-PDA/E51 ratios of 7-16 wt.% were prepared and subjected to four different curing process and time combinations, followed by the characterization of their compressive properties. According to the slope for a plot of the compressive strength versus strain for the epoxy resin, when the slope of the curve remained unchanged with increasing strain, the epoxy resin was in the elastic deformation stage. When the slope was negative, the strain of the epoxy resin was in the softening stage. When the slope increased gradually with the increasing strain of the epoxy resin, the epoxy resin was in the strain strengthening stage. The compression characteristics of the epoxy resins at each curing process were analyzed separately.

Under curing process (I) (4 h at 60 °C and 20 h at 80 °C), the epoxy resins exhibited strain softening behavior after yield, except for those with *m*-PDA/E51 ratios of 12 wt.% and 13 wt.%, which did not enter the strain hardening stage before failure. As shown in Figs. 3(a) and 3(b), the stress enhancement amplitudes for these ratios were significantly smaller than those observed under curing processes (II), (III), and (IV). This suggests that the reaction between the epoxy resin and *m*-PDA had not fully completed, resulting in lower cross-linking and weaker material performance under curing process (I).

Figs. 3(a) and 3(d) indicate that the compressive strengths of the epoxy resins first increased and then decreased with increasing *m*-PDA/E51 ratio. When the *m*-PDA/E51 ratio was 12 wt.%, the yield strength peaked at 144.63 MPa (compressive strain of 37.67%). The yield strain of the epoxy resin showed an upward trend with increasing *m*-PDA dosage, but in a relatively small range mainly between 6-8%. As displayed in Fig. 3(c), the Young's modulus exhibited a downward trend with increasing amounts of *m*-PDA from 8 to 16 wt.%. When

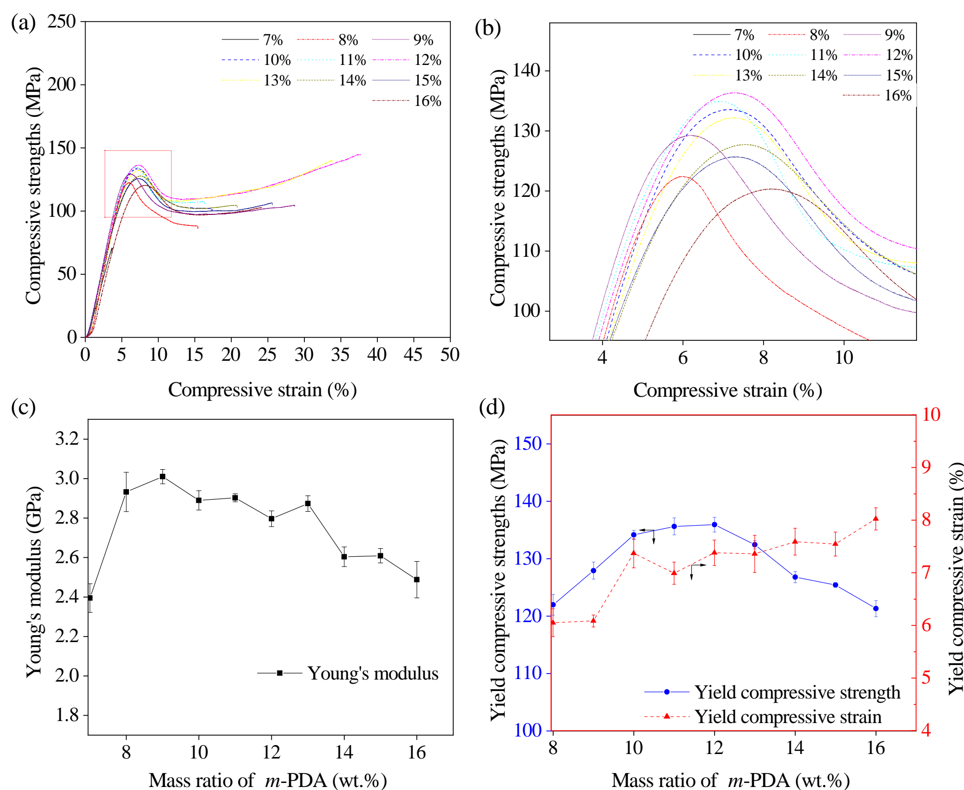

Fig. 3. Mechanical properties of epoxy resins cured under process (I). (a) compressive strength-strain curves, (b) magnification, (c) Young's modulus and (d) yield compressive strengths-strain.

the amount of *m*-PDA was 7 wt.%, the Young's modulus was the lowest, attributed to an insufficient degree of the curing reaction.

For curing process (II) (4 h at 80 °C, 2 h at 150 °C and 3 h at 180 °C), the epoxy resins with *m*-PDA/E51 ratios of 7 and 8 wt.% showed obvious strain softening stages and yield turning points (Figs. 4(a) and 4(b)). The epoxy resins with *m*-PDA/E51 ratios of 9-16 wt.% exhibited lower strain softening stages (Lin et al., 2016). The toughness and strength gradually increased without obvious yield turning points. Therefore, it is reasonable to conclude that the *m*-PDA dosage had a significant impact on the extent of epoxy resin curing. When the *m*-PDA/E51 ratios were 9-16 wt.%, the reactions of the epoxy resins progressed further and they produced higher cross-linking densities; however, the epoxy resins with *m*-PDA/E51 ratios of 7-8 wt.% showed insufficient curing and low cross-linking densities. As shown in Fig. 4(c), with an increasing amount of *m*-PDA used, the Young's modulus of the epoxy resins showed a downward trend. The epoxy resins with *m*-PDA/E51 ratios of 9-16 wt.% did not exhibit obvious yield turning points, and the maximum strains of the epoxy resins were greater than 20%. Thus, the compressive strengths corresponding to 10% and 20% strain were used to compare the strengths of the epoxy resins. Fig. 4(d) illustrates that when the strain was 10%, the compressive strengths of the epoxy resins were the highest at 134.10 MPa when the *m*-PDA/E51 ratio was 8 wt.%. When the strain was 20%, the compressive strengths were relatively consistent for *m*-PDA/E51 ratios between 11 wt.% and 13 wt.%, stabilizing around 149 MPa. The compressive strengths peaked at 149.40 MPa when the *m*-PDA/E51 ratio was 12 wt.%.

For curing process (III) (3.5 h at 50 °C, 12 h at 80 °C and 3.5 h at 180 °C), the epoxy resins with *m*-PDA/E51 ratios of 7, 8 and 9 wt.% had obvious yield turning points, while the epoxy resins with other *m*-PDA/E51 ratios showed no obvious yield turning points. Figs. 5(a) and 5(b) show that the compressive strength and strain of the epoxy resin were relatively high, indicating that the curing reaction was more complete with curing process (III) and the cross-linking network was relatively dense.

As the *m*-PDA/E51 ratio increased, the Young's modulus of the epoxy resins gradually decreased, as illustrated in Fig. 5(c). Epoxy resins with *m*-PDA/E51 ratios between 10 wt.% and 16 wt.% did not exhibit clear yield turning points. To compare the mechanical properties of these resins, their compressive strengths at 10% and 20% strains were evaluated. Under a compressive strain of 10%, the compressive strength of the epoxy resins initially increased, reaching a peak of 132.48 MPa when the *m*-PDA/E51 ratio was 8 wt.%. Subsequently, the strength decreased and stabilized around 12 wt.% *m*-PDA/E51 ratio. Fig. 5(d) illustrates that under a compressive strain of 20%, the compressive strength followed a similar trend: it initially increased and then decreased with increasing *m*-PDA/E51 ratio. The maximum compressive strength of 147.72 MPa was observed at an *m*-PDA/E51 ratio of 11 wt.%, with a slightly lower strength of 147.10 MPa recorded at 12

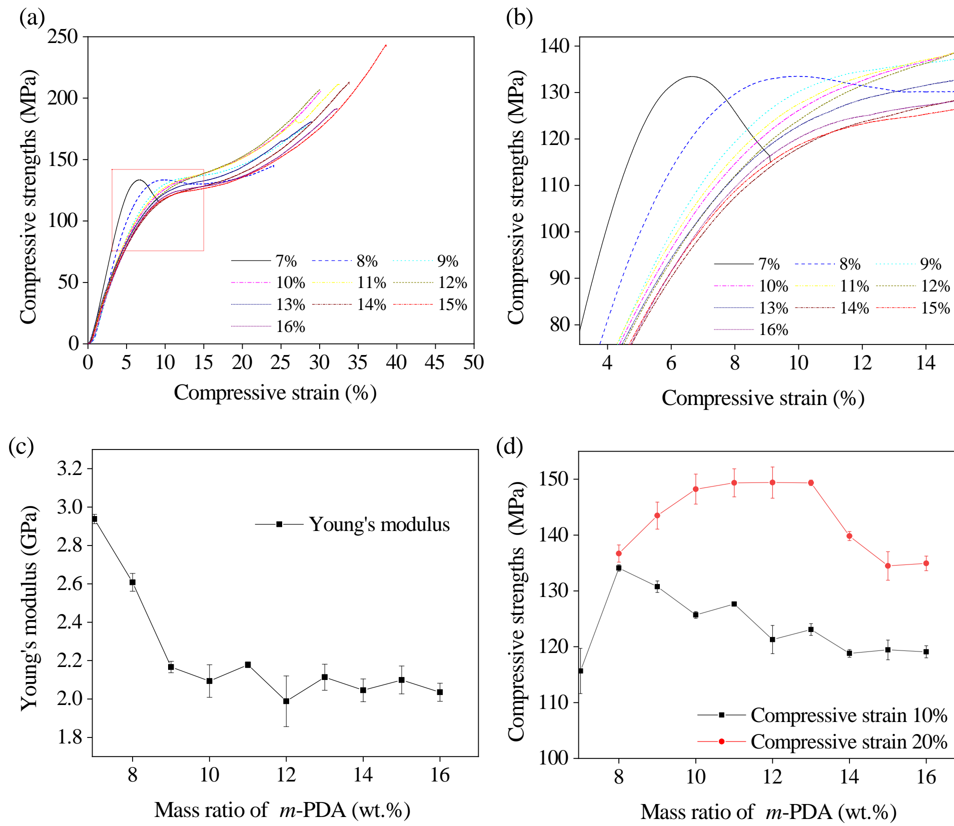

Fig. 4. Mechanical properties of epoxy resins cured under process (II). (a) compressive strength-strain curves, (b) magnification, (c) Young's modulus and (d) compressive strength under strains of 10% and 20%.

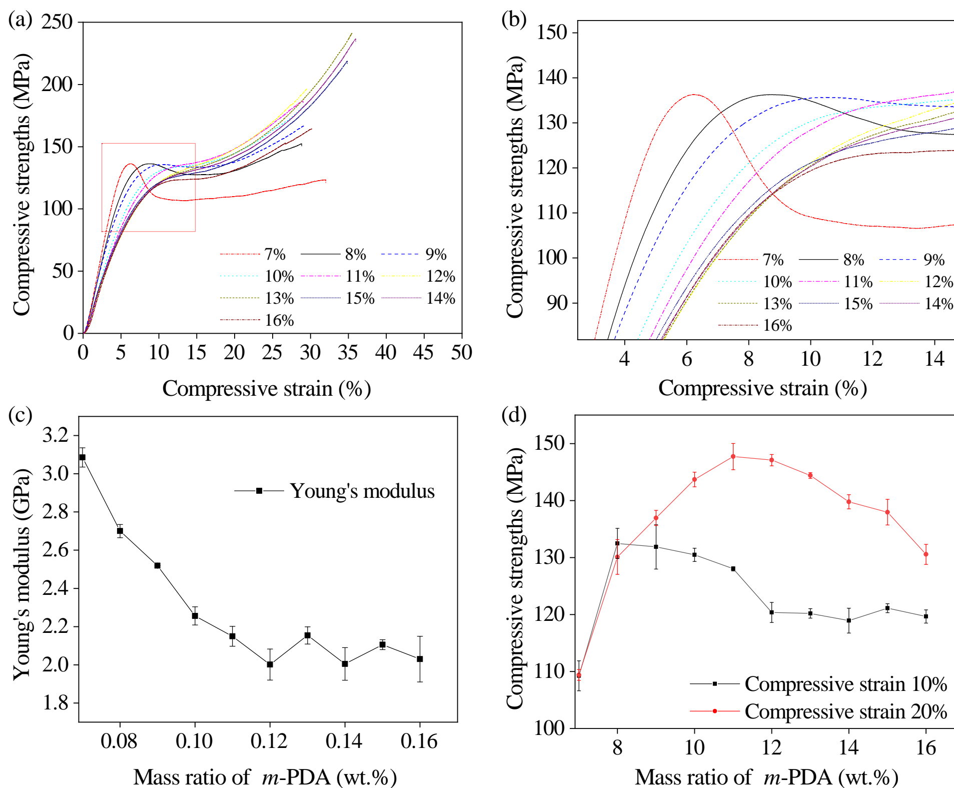

Fig. 5. Mechanical properties of epoxy resins cured under process (III). (a) compressive strength-strain curves, (b) magnification, (c) Young's modulus and (d) compressive strength under strains of 10% and 20%.

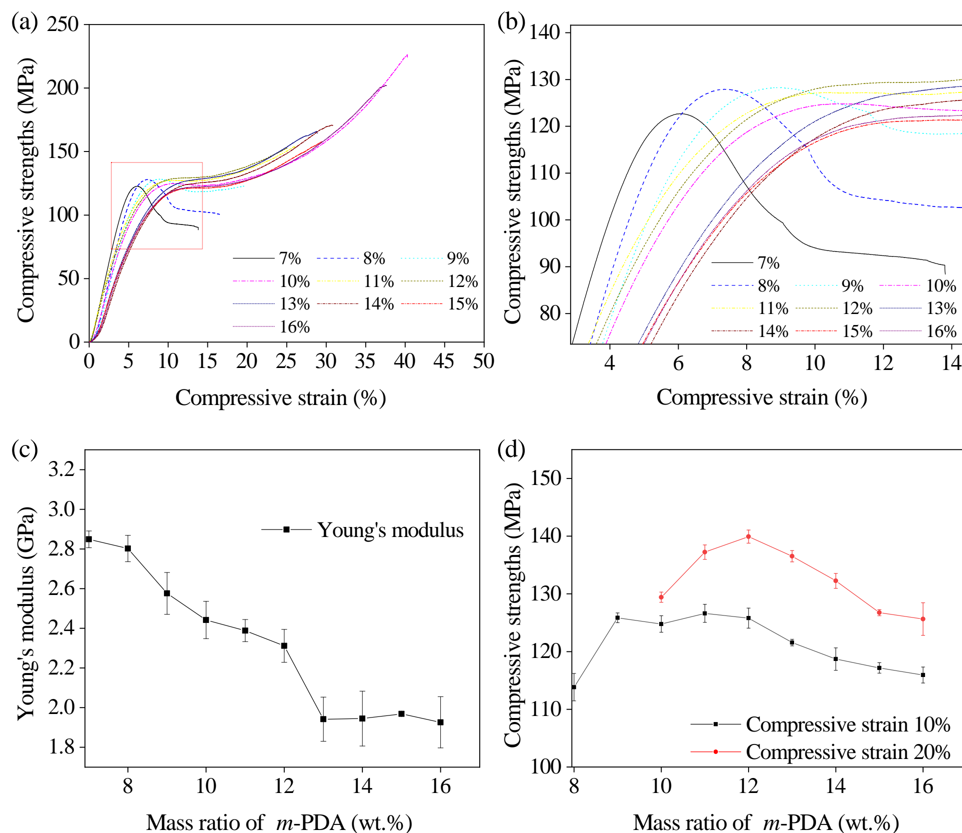

Fig. 6. Mechanical properties of epoxy resins cured under process (IV). (a) compressive strength-strain curves, (b) magnification, (c) Young's modulus and (d) compressive strength under strains of 10% and 20%.

wt.%.

For curing process (IV) (3.5 h at 50 °C and 2 h at 80 °C), the yield turning points were obvious when the *m*-PDA/E51 ratios were 7-10 wt.%, as shown Figs. 6(a) and 6(b). Moreover, the epoxy resins with *m*-PDA/E51 ratios of 7 and 8 wt.% were always in the strain softening stage after yielding, and there were no strain hardening phenomena observed before the samples were destroyed. When the *m*-PDA/E51 ratios were 11-16 wt.%, there was no obvious yield turning point and the samples entered a "plateau stage" (the compressive strength was almost constant with increasing strain) after elastic deformation. At the end of this stage, strain hardening occurred until the samples degraded. Fig. 6(c) confirms that the Young's modulus of the epoxy resins gradually decreased with increasing *m*-PDA/E51 ratio, and the Young's modulus gradually stabilized when the amount of *m*-PDA reached 13 wt.%.

As the *m*-PDA/E51 ratio increased from 7 to 9 wt.%, the yield strengths and strains of the epoxy resins gradually increased, indicating an enhancement in both toughness and strength with the addition of *m*-PDA. However, for epoxy resins with *m*-PDA/E51 ratios between 11 and 16 wt.%, where no obvious yield turning points were observed, the mechanical properties were compared under compressive strains of 10% and 20%. Under a compressive strain of 10%, the compressive strength initially increased and then decreased as the *m*-PDA/E51 ratio increased, with the highest value of 126.62 MPa observed at an *m*-PDA/E51 ratio of 11 wt.%. Similarly, under a compressive strain of 20%, the compressive strength followed a similar trend, peaking at 139.92 MPa when the *m*-PDA/E51 ratio was 12 wt.%. These results, shown in Fig. 6(d), demonstrate the variation in compressive strength with changes in the *m*-PDA/E51 ratio, illustrating the influence of *m*-PDA on the mechanical properties of the epoxy resins.

In the mechanical experiments, the four classes of epoxy resins treated with different curing processes generally exhibited the same behaviors. As the ratio of *m*-PDA/E51 increased, the slopes for the elastic deformation sections of the compressive stress-strain curves for epoxy resins, namely, the Young's modulus, showed downward trends. When the amount of *m*-PDA added was small, the strain of epoxy resin at failure was relatively low, the yield compressive strength was relatively high, and the corresponding yield compressive strain was comparatively small. Therefore, the epoxy resins with relatively low *m*-PDA/E51 ratios were hard and brittle. When the *m*-PDA/E51 ratio was high, the final compressive strain of the epoxy resins was relatively large, they did not show an obvious yield turning point, and their maximum compressive strength was high. Therefore, the epoxy resins with relatively high *m*-PDA/E51 ratios were hard and tough.

For different curing processes, the compressive strengths reached their maximum values under the same compressive strain when the *m*-PDA dosages were 11-13 wt.% (epoxy resins cured at curing process (I) were compared within the

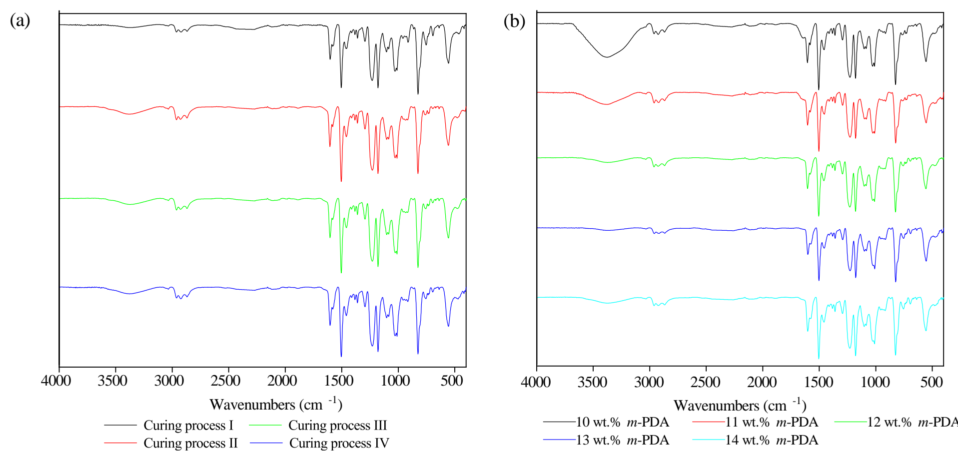

Fig. 7. IR absorption spectra of the epoxy resins under (a) different curing processes, 12 wt.% *m*-PDA and (b) different ratios of *m*-PDA, curing process (III).

yield strength), which were slightly lower than the theoretical dosage of 13 wt.%. The reason is that, during the actual curing process, the reactive functional groups of the *m*-PDA molecule and the E51 molecule cannot fully contact each other (D'Almeida and Monteiro, 1996). This is mainly due to the high steric hindrance of E51 molecules and the increased viscosity of the system caused by the curing reaction, which affects the free diffusion of *m*-PDA molecules in the system and results in the failure to form a theoretical cross-linked curing network (Okabe et al., 2016). In addition, the *m*-PDA molecule acting as a plasticizer is not conducive to the enhancement of resin strength.

In order to obtain the optimal compressive strength of the epoxy resins, the mass ratios of *m*-PDA to E51 were 11-13 wt.%, and the optimal curing process was (III) with 3.5 h/50 °C, 12 h/80 °C, and 3.5 h/180 °C.

3.5.2 Infrared absorption spectra

The absorption bands in the FTIR spectra provide valuable information on the presence of specific chemical bonds and functional groups, allowing for the determination of the degree of epoxy resin curing. In the curing process, one NH_2 functional group of *m*-PDA can react with two epoxide groups in the epoxy resin. The optimum theoretical *m*-PDA/E51 ratio is 13 wt.%, while due to steric hindrance and other factors affecting the curing reactions, a small excess of E51 is often added to ensure a complete reaction with *m*-PDA. The curing reaction between epoxy E51 and *m*-PDA involves two steps. First, the primary amines (-NH_2) of *m*-PDA initiate nucleophilic addition to the epoxide groups, causing the epoxide rings to open and forming secondary alcohols and secondary amines. In the second step, the secondary amines react with another epoxy group of bisphenol A glycidyl ether. This process leads to the attachment of four R groups (where each R represents the reacted groups of the E51 monomers) to each *m*-PDA molecule, with each R group consisting of two *m*-PDA molecules. As a result, numerous cross-linking networks are formed within the epoxy resin, and the obtained complex cross-linking structure, along with the rigid benzene rings, imparts high strength to this material.

Taking curing process (III) and a 12 wt.% ratio of *m*-PDA/E51 as an example, the FTIR spectra revealed various functional groups in the epoxy resin, and the absorption peaks associated with different chemical bonds were observed within specific wavenumber ranges. For the benzene ring groups, peaks appeared at 780-910 cm^{-1} (γ_{C-H}), 1,410-1,685 cm^{-1} ($\upsilon_{C=C}$) and 2,750-3,000 cm^{-1} (υ_{C-H}). The ether bond was characterized by peaks at 970-1,060 cm^{-1} (υas_{C-O-C}) and 1,190-1,275 cm^{-1} (vas_{C-O-C}), while the alcoholic hydroxyl group exhibited peaks at 420-620 cm^{-1} (γ_{O-H}), 1,270-1,370 cm^{-1} (σ_{O-H}) and 3100-3645 cm^{-1} (υ_{O-H}), with the latter being broad due to significant hydrogen bond association. Additional peaks for secondary alcohols were observed at 1,058-1,145 cm^{-1} (υ_{C-O}). Furthermore, the presence of C=C bonds (produced by hydrolysis) was indicated by peaks at 670-710 cm^{-1} (γ_{C-H}) and 3,000-3,080 cm^{-1} (υ_{C-H}). The C-N bond was identified at 1,370-1,400 cm^{-1} (υ_{C-N}), and the N-H bond appeared at 3,250-3,350 cm^{-1} (υ_{N-H}). Finally, the epoxide group was confirmed by a peak at 715-780 cm^{-1} (υ_{C-O-C}).

Next, the analyses of the infrared data were performed for epoxy resins with the same *m*-PDA/E51 ratios but different curing processes. Fig. 7(a) confirms that the absorption peaks in the FTIR spectra for the four epoxy resins obtained from four different curing processes were basically the same, indicating that the epoxy resins underwent the same curing reactions. Nevertheless, obvious absorption peaks appeared at 715-780 cm^{-1} (ν_{C-O-C}) for curing processes (I) and (IV), which indicated that the epoxy groups of E51 did not react completely with the primary amines of *m*-PDA at these two curing processes, hence epoxide groups still remained in the curing system. The four epoxy resins cured at different temperatures showed absorption peaks at 3,400 cm^{-1} (ν_{N-H} and ν_{O-H}). The absorption peaks for curing processes (I) and (IV) were more obvious. Combined with the absorption peaks at 750 cm^{-1}, this indicated that the primary amine groups of *m*-PDA had not reacted completely with the epoxy groups after the system had been cured with curing processes (I) and (IV). As a result, more -NH_2 groups remained unreacted. Compared with (I) and (IV), curing protocols (II) and (III) had periods

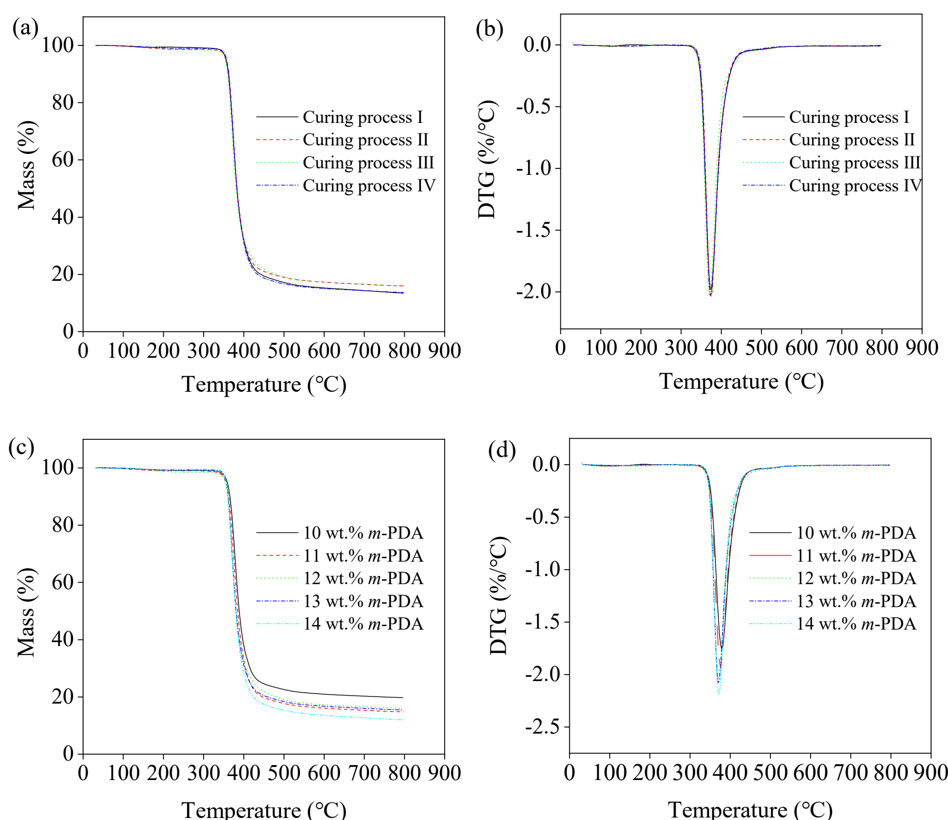

Fig. 8. TG-DTG curves for the epoxy resins at (a) different curing temperatures, 12 wt.% *m*-PDA, (b) different curing temperatures, 12 wt.% *m*-PDA, (c) different ratios of *m*-PDA, curing process III and (d) different ratios of *m*-PDA, curing process (III).

Table 3. Thermal decomposition temperatures and char yield of epoxy resins with different curing process.

Process	Temperature (°C)			Char yield (wt.%)
	Initial	Peak	Final	
I	359.3	374.0	398.4	13.45
II	360.0	374.6	387.8	15.96
III	357.8	370.5	392.6	15.95
IV	359.5	373.4	398.2	13.71

of high-temperature curing (180 °C), which indicated that the high-temperature curing process had a significant effect on the reactions of epoxy resins.

Next, the analyses of infrared results were performed for epoxy resin with different *m*-PDA ratios but cured at the same curing process. Fig. 7(b) illustrates that the absorption peaks in the FTIR spectra of epoxy resins with different *m*-PDA/E51 ratios were basically the same in the low wavenumber range. However, in the high wavenumber range (approximately 3400 cm^{-1}), the epoxy resins with *m*-PDA/E51 ratios of 10, 11 and 14 wt.% showed more obvious absorption peaks than resins treated with 12 and 13 wt.% *m*-PDA. The epoxy resin with an *m*-PDA/E51 ratio of 10 wt.% had the largest absorption peak area. Since the dosage of *m*-PDA was too low in this case, the extent of cross-linking was also low and the distribution was not uniform. The hydrogen bonds of the epoxy resin treated with this *m*-PDA dosage were more likely to be associated with each other on a large scale, which enhanced the intensity of the band for hydroxyl groups (ν_{O-H}). As the dosage of *m*-PDA was increased and it approached the theoretical amount for *m*-PDA (13 wt.%), the extent of epoxy group cross-linking increased, the associations between hydroxyl groups weakened and the peak intensities for the epoxy resin decreased in this infrared spectral region.

3.5.3 Thermal stability

Using the method of intersecting external tangent lines, the initial thermal decomposition temperature, peak thermal decomposition temperature, and final thermal decomposition temperature were obtained as shown in Fig. 8(a). According to Fig. 8(b), the peak temperature corresponding to the maximum absolute value of DTG was obtained, and the temperature data are summarized in Table 3. The initial temperature, peak temperature and end temperature were similar for the thermal decompositions of epoxy resins made at different curing processes, suggesting that the thermal stabilities of the chemical bonds were similar for cured epoxy resins made at different curing processes. However, the proportions of carbon residues in samples made at curing process (II) and (III) were

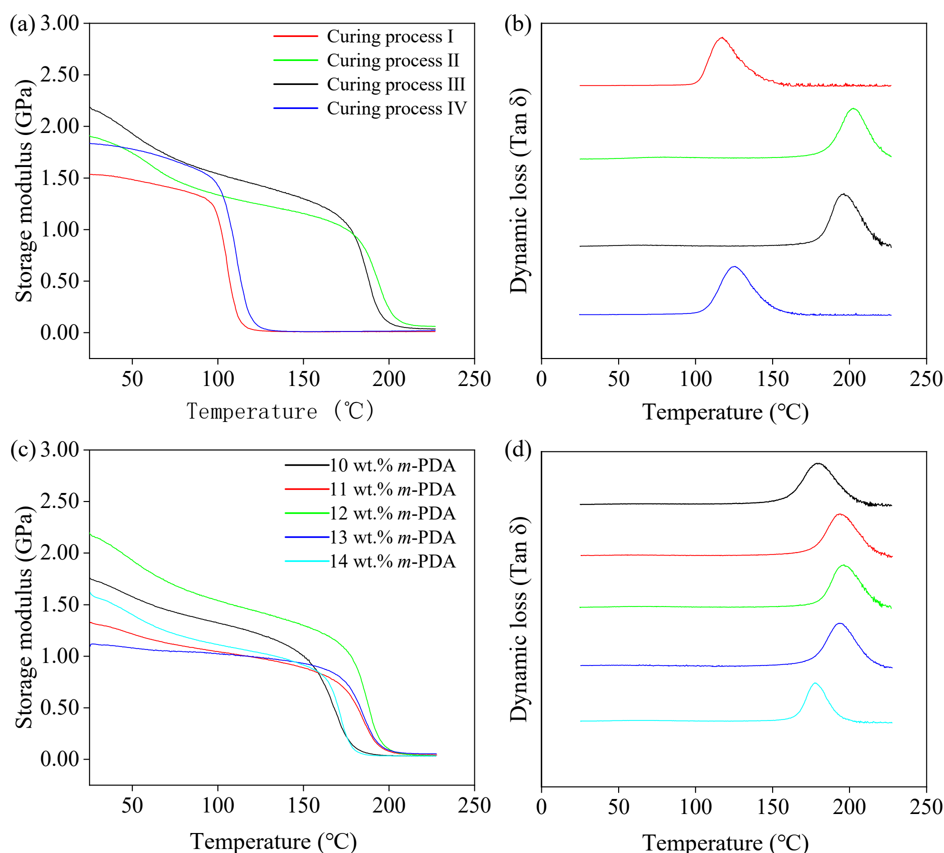

Fig. 9. Thermal dynamic mechanical properties of epoxy resins. (a) Curing by different processes, 12 wt.% *m*-PDA, (b) curing by different processes, 12 wt.% *m*-PDA, (c) different ratios of *m*-PDA/E51, curing process (III) and (d) different ratios of *m*-PDA/E51, curing process (III).

Table 4. Thermal decomposition temperatures and char yield of epoxy resins with different m-PDA ratios.

m-PDA/E51 ratio (wt.%)	Temperature (°C)			Char yield (wt.%)
	Initial	Peak	Final	
10	360.8	377.9	402.6	19.77
11	359.0	375.8	400.2	14.75
12	357.8	370.5	392.6	15.95
13	356.3	370.6	394.5	15.42
14	358.2	371.3	394.7	11.99

higher than those made at curing processes (I) and (IV).

For curing process (III), the thermal decomposition temperatures of the epoxy resins made with different m-PDA/E51 ratios are summarized in Table 4, Figs. 8(c) and 8(d). The results suggest that the thermal stabilities of epoxy resins cured with different *m*-PDA/E51 ratios were similar. With increasing *m*-PDA dosage, the char yield shows a downward trend.

We can conclude that the thermal decomposition temperature of epoxy resins from various processes is significantly higher than the working temperature (150 °C). Therefore, the epoxy resins prepared in this study remain stable at the working temperature and are not subject to thermal decomposition.

3.5.4 Dynamic thermomechanical properties

The glass transition temperatures (Tg) of epoxy resins cured according to curing processes (I) and (IV) were 117.9 and 125.1 °C, respectively, as illustrated in Fig. 9(a) and 9(b). These values were lower than those of the resins cured under curing processes (II) and (III), which had Tg values of 203.0 and 196.7 °C, respectively. The degree of cross-linking in epoxy resin plays a key role in determining its Tg. As the degree of cross-linking increases, the entanglement between molecular chains also increases, requiring higher temperatures for relaxation motions. This indicates that the high-temperature curing stage significantly influences the curing degree and mechanical properties of the epoxy resins.

Under curing process (III) and a 12 wt.% *m*-PDA/E51 ratio, the energy storage modulus and glass Tg of the epoxy resins reached their highest values. This observation, as supported by Figs. 9(c) and 9(d), indicates that the optimal *m*-PDA/E51 ratio was 12 wt.% when combined with the actual curing reaction. The Tg values of the epoxy resins were categorized into three levels: 1) 12 wt.% (196.7 °C); 2) 11 wt.% (193.6 °C), 13 wt.% (194.0 °C); 3) 14 wt.% (179.6 °C), and 10 wt.% (177.5 °C). These data suggest that the Tg of the epoxy resin is higher when the *m*-PDA/E51 ratio approaches 12 wt.%.

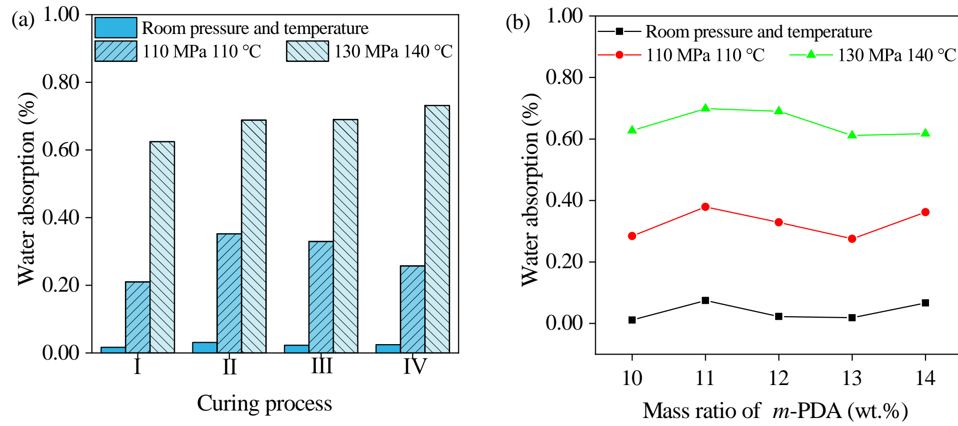

Fig. 10. Water absorption of epoxy resins under (a) curing by different processes, 12 wt.% and (b) different ratios of *m*-PDA/E51, curing process (III).

The storage modulus of the epoxy resins, as illustrated in Figs. 9(c), exhibited an initial increase followed by a decrease with an increasing *m*-PDA/E51 ratio. This behavior can be attributed to the small deformation conditions under which the storage modulus is measured using DMA. In this scenario, the interactions between chain segments in the epoxy resin are not disrupted and the distances between chain segments remain unchanged due to the cross-networked structure of the resin. The modulus at this stage depends on the cross-linking density and the amount of uncross-linked *m*-PDA in the system. The residual *m*-PDA acts as a small molecule plasticizer, reducing the modulus of the epoxy resin. Therefore, the combined effects of high cross-linking density and the plasticizing action of residual *m*-PDA result in the observed trend of storage modulus first increasing and then decreasing with additional *m*-PDA present. In mechanical experiments assessing compressive strength, different patterns were seen due to the distinct deformation scales involved. For instance, in compressive strength tests, the strain reached 5%, with a shape variable exceeding 10,000 μm under uniaxial load, maintaining stability in a single direction. Conversely, the DMA test involves a sinusoidal load and a shape variable of less than 10 μm, which led to different outcomes for modulus behavior (Du et al., 2021; Thirumalai et al., 2019).

3.5.5 Resistance of epoxy resins to high-temperature and high-pressure water environments

The thermal insulation material used for the deep ICP-coring device is designed to operate in a high-temperature and high-pressure water environment. Therefore, for the matrix of the thermal insulation material, the tolerance of the epoxy resin to high-temperature and high-pressure water is essential. The epoxy resins were set for 4 h within a container with a high-temperature and high-pressure water environment provided by the temperature-preserved coring comprehensive test platform, which was developed in our laboratory. The water absorption rate was measured and used to judge the performance of the epoxy resins to withstand high-temperature and high-pressure water environments.

Fig. 10 shows that epoxy resins basically do not absorb water at atmospheric temperature and pressure. Under a high-temperature and high-pressure water environment, water absorption by epoxy resins is also relatively low, with the highest value being no more than 0.7%. The curing process and *m*-PDA dosage seem to have little effect on water absorption by epoxy resins, and the amount of water absorbed by epoxy resin increases with rising temperature and pressure of the water environment. This is because the higher the temperature is, the more intense the thermal motion of water molecules and epoxy resin chain segments; with higher pressure, it is easier for water molecules to enter the chain segment gaps of the epoxy resin.

3.5.6 Insulation performance

The thermal conductivity of epoxy resin is approximately 0.25 W/m·K, which is relatively low compared to materials like 304 stainless steel (16.2 W/m·K), marble (2.7 W/m·K) and glass (0.7 W/m·K). As shown in Fig. 11, the curing temperature and *m*-PDA/E51 ratio have minimal effects on the thermal conductivity of the resin. In non-conducting solids, heat is primarily transferred through lattice vibrations (phonons) (Tao, 2019). Due to the elongated chain structure of epoxy resin, weak intermolecular forces between molecular chains, and its distinctive vibrational characteristics, energy transfer between molecules relies on specific vibrational modes and collisions. This leads to increased phonon scattering, which limits phonon transport and results in the low thermal conductivity of the epoxy resin.

In order to characterize the temperature preservation performance of the thermal insulation material section of the passive thermal insulation system for the high-temperature rock core, the simulated structural parts of the core cabin were designed and manufactured according to the size of the deep ICP-coring device. Structural part I was used for the passive insulation material epoxy resin and structural part II was used for the blank control experimental group, as shown in Figs. 12(a) and 12(b), respectively. Structural part I has an annulus of 618 mL capacity for injecting passive insulation material, and a thermal insulation layer with a thickness of 6.55 mm to enhance temperature control. The annulus part of structural

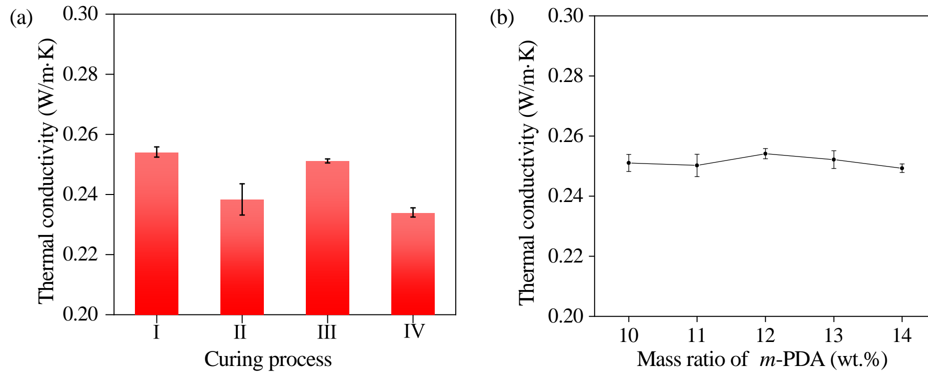

Fig. 11. Thermal conductivity of the epoxy resins. (a) Different curing processes, 12 wt.% *m*-PDA and (b) different ratios of *m*-PDA/E51, curing process (III).

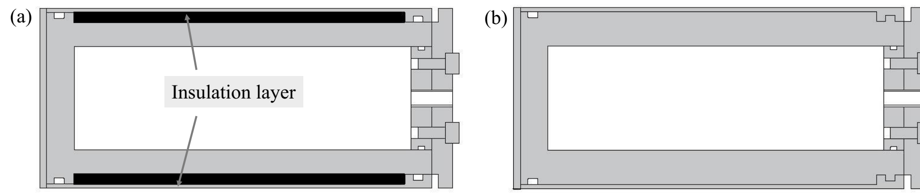

Fig. 12. The structural part for testing the insulation performance of the passive thermal insulation system: (a) Structural part I and (b) structural part II.

part II is made from steel, and the remaining dimensions are the same as those of structural part II.

In the experimental process, first, epoxy resin was injected into the annulus of structural part I, and after a curing process III, heat conduction oil was loaded into the inner cylinder of the structural parts. The tooling was then placed in an oven at 150 °C, and heating was stopped once the temperature of the oil stabilized at 150 °C. Afterwards, the structural parts were removed from the oven and placed at room temperature. The temperature change curves of the experimental group and the control group were recorded. The test was performed 3 times, and the results are shown in Fig. 13. The temperature change of the simulated core in the experimental group was slower than that in the control group during the heating and cooling process of the structural tooling. This confirms that the insulation material epoxy resin can reduce the heat exchange between the core and the outside world. Once the temperature of the simulated core in the experimental group reached 150 °C, the structural parts were cooled down. Under the conditions of room temperature (25 °C) and wind speeds of 0, 3 and 6 m/s, the experimental group reduced heat exchange between the simulated core and the external environment by 19.01%, 18.36% and 13.17%, respectively, within 1 hour after the cooling started. Within 2 hours, the experimental group reduced heat exchange by 11.76%, 12.57% and 8.89%, and within 5 hours, the reduction was 7.50%, 5.79% and 4.76%, respectively, compared to the control group.

4. Conclusions

In this work, a passive insulation system for a deep ICP-coring device was designed, and high-strength epoxy resin, capable of withstanding deep high-temperature and high-pressure environments, was developed as its insulation material. The key findings are summarized as follows:

1) The passive insulation system comprises a vacuum layer and a passive insulation material layer. The core cabin sleeve section utilizes a vacuum layer, while other sections of the core cabin employ a passive insulation layer.
2) The *m*-PDA-E51 epoxy resin system was selected as the insulation material for the passive insulation system, with an optimized *m*-PDA/E51 dosage of 11–13 wt.% and curing conditions of 3.5 h at 50 °C, 12 h at 80 °C, and 3.5 h at 180 °C. Under these conditions, the epoxy resin achieved a compressive strength of 241.03 MPa, a glass transition temperature of 203.0 °C, and an initial thermal decomposition temperature of approximately 360 °C.
3) The epoxy resin minimized heat exchange between the core and the external environment by up to 19.01%, meeting the strength requirements without increasing the device's size.

Acknowledgements

This work was supported by the National Natural Science Foundation of China (Nos. 52304033, 51827901), the Sichuan Science and technology Program (No. 2023NSFSC0790), and the Sichuan University Postdoctoral Fund (No. 2024SCU12093).

Conflict of interest

The authors declare no competing interest.

Open Access This article is distributed under the terms and conditions of the Creative Commons Attribution (CC BY-NC-ND) license, which permits unrestricted use, distribution, and reproduction in any medium, provided the original work is properly cited.

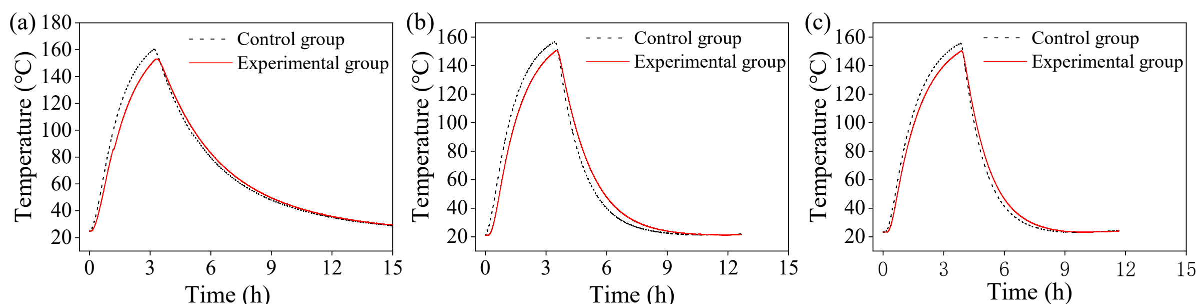

Fig. 13. Temperature-time curves of simulated cores at 25 °C under different heat transfer conditions: (a) Wind Speed 0 m/s, (b) Wind Speed 0 m/s and (c) Wind Speed 6 m/s.

References

D'Almeida, J., Monteiro, S. The effect of the resin/hardener ratio on the compressive behavior of an epoxy system. Polymer Testing, 1996, 15(4): 329-339.

Du, U. L. N., Bethke, C., Altstaedt, V., et al. New insights on expandability of pre-cured epoxy using a solid-state co_2-foaming technique. Polymers, 2021, 13(15): 2441-2463.

El Gazzani, S., Nassiet, V., Habas, J.-P., et al. High temperature epoxy foam: Optimization of process parameters. Polymers, 2016, 8(6): 215-233.

Hossain, M. E. Drilling costs estimation for hydrocarbon wells. Journal of Sustainable Energy Engineering, 2015, 3(1): 3-32.

Inada, N., Koji, Y. Data report: Hybrid Pressure Coring System tool review and summary of recovery result from gas-hydrate related coring in the Nankai Project. Marine & Petroleum Geology, 2015, 66(2): 323-345.

Kong, L., Xie, H., Li, C. Coupled microplane and micromechanics model for describing the damage and plasticity evolution of quasi-brittle material. International Journal of Plasticity, 2023, 162: 103549.

Kumar, A., Srivastava, A. Preparation and mechanical properties of jute fiber reinforced epoxy composites. Industrial Engineering & Management, 2017, 6(234): 2169-0316.

Liang, B., Gao, H., Lan, Y. Theoretical analysis and experimental study on relation between roack permeabikity and temperature. Chinese Journal of Rock Mechanics and Engineering, 2005, 24(12): 2009-2012. (in Chinese)

Lin, S., Huang, Y., Xie, D., et al. Molecular relaxation and glass transition properties of epoxy resin at high temperature. Acta Physica Sinica, 2016, 65(07): 304-310.

Moller, J. C., Berry, R. J., Foster, H. A. On the nature of epoxy resin post-curing. Polymers, 2020, 12(2): 466.

Okabe, T., Oya, Y., Tanabe, K., et al. Molecular dynamics simulation of crosslinked epoxy resins: Curing and mechanical properties. European Polymer Journal, 2016, 80: 78-88.

Saif, T., Lin, Q., Bijeljic, B., et al. Microstructural imaging and characterization of oil shale before and after pyrolysis. Fuel, 2017, 197: 562-574.

Shi, X., Li, J., Li, C., et al. Design and strength analysis of the passive thermal insulation structure of a deep rock *in-situ* thermal insulation coring system. Thermal Science, 2023, 27(1B): 1-8.

Tao, W. Q. Heat Transfer (The fifth edition). Beijing, P. R. China, Higher Education Press, 2019. (in Chinese)

Thirumalai, R., Prakash, R., Ragunath, R., et al. Experimental investigation of mechanical properties of epoxy based composites. Materials Research Express, 2019, 6(7): 075309.

Vashisth, A., Ashraf, C., Bakis, C. E., et al. Effect of chemical structure on thermo-mechanical properties of epoxy polymers: Comparison of accelerated ReaxFF simulations and experiments. Polymer, 2018, 158: 354-363.

Wang, H., Huang, H., Bi, W., et al. Deep and ultra-deep oil and gas well drilling technologies: Progress and prospect. Natural Gas Industry B, 2022, 9(2): 141-157.

Xie, H., Gao, M., Zhang, R., Zhou, H., et al. Application prospects of deep *in-situ* condition-preserved coring and testing systems. Advances in Geo-Energy Research, 2024, 14(1): 12-24.

Xie, H., Liu, T., Gao, M., et al. Research on *in-situ* condition preserved coring and testing systems. Petroleum Science, 2021, 18(6): 1840-1859.

Xue, Y., Wang, J., Xiao, J. Bibliometric analysis and review of mine ventilation literature published between 2010 and 2023. Heliyon, 2024, 10(4): e26133.

Yang, J., Chen, L., Gu, X., et al. Hollow glass microspheres/silicone rubber composite materials toward materials for high performance deep *in-situ* temperature-preserved coring. Petroleum Science 2021, 19(1): 309-320.

Zhang, Y., Sun, J., Zhao, H., et al. Test research on *in-situ* sampler for gas hydrate. Exploration Engineering (Rock & Soil Drilling and Tunneling), 2007, 34(9): 62-65. (in Chinese)

Zhao, J., Yang, D., Kang, Z., et al. A micro-CT study of changes in the internal structure of Daqing and Yan'an oil shales at high temperatures. Oil Shale, 2012, 29(4): 357.

Zhou, X., Pang, X., Li, Q., et al. Advances and problems in hydrocarbon exploration in the Tazhong area, Tarim Basin. Petroleum Science, 2010, 7(2): 164-178.

Zhu, H., Liu, Q., Wong, G., et al. A Pressure and Temperature Preservation System for Gas-hydrate-bearing Sediments Sampler. Petroleum Science and Technology, 2013, 31(6): 652-662.